

The Source of Hydrogen in Earth's Building Blocks

Thomas J. Barrett¹, James F.J. Bryson¹, Kalotina Geraki²

1. Department of Earth Sciences, University of Oxford, Oxford, OX1 3AN, UK.
2. Diamond Light Source, Harwell Science and Innovation Campus, Didcot, OX11 0DE, UK.

Email: thomas.barrett@st-annes.ox.ac.uk

Abstract

Despite being pivotal to the habitability of our planet, the process by which Earth gained its present-day hydrogen budget is unclear. Due to their isotopic similarity to terrestrial rocks across a range of elements, the meteorite group that is thought to best represent Earth's building blocks is the enstatite chondrites (ECs). Because of ECs' nominally anhydrous mineralogy, these building blocks have long been presumed to have supplied negligible hydrogen to the proto-Earth. However, recent bulk compositional measurements suggest that ECs may unexpectedly contain enough hydrogen to readily explain Earth's present-day water abundance. Together, these contradictory findings mean the contribution of ECs to Earth's water budget is currently unclear. As such, it is uncertain whether appreciable water is a systematic outcome of Earth's formation. Here, we explore the amount of hydrogen in ECs as well as the phase that may carry this element using sulfur X-ray absorption near edge structure (S-XANES) spectroscopy. We find that most (~80 wt%) of the measured bulk hydrogen concentration of these meteorites is bonded to sulfur. Moreover, the concentration of the S-H bond is intimately linked to the abundance of micrometre-scale pyrrhotite (Fe_{1-x}S , $0 < x < 0.125$), suggesting most hydrogen in these meteorites is carried in this phase. These findings indicate that hydrogen is present in ECs in higher concentrations than previously considered and argue this element has a systematic, rather than stochastic, origin on our planet.

Key Words

Meteorites, Planetary formation, Cosmochemistry

Introduction

Although water is central to planetary habitability as we know it, the mechanism by which Earth gained its substantial present-day water budget is unclear. Enstatite chondrites (ECs) closely resemble terrestrial rocks across a range of isotopic compositions (Dauphas, 2017). Hence, ECs (or material similar to these meteorites) have been suggested as the predominant building blocks of the proto-Earth (Javoy et al., 2010), as well as other terrestrial planets including Mars (Brasser et al., 2018). ECs formed in the hot inner solar system, so consist entirely of nominally anhydrous minerals (Weisberg & Kimura, 2012). As such, Earth's building blocks have long been presumed to have been 'dry', and so provided negligible water to the proto-Earth (Marty, 2012; Morbidelli et al., 2000). This concept has recently been reinforced by measurements of very low water concentrations in nominally anhydrous silicates in aubrites (melted ECs) (Peterson et al., 2023), which may have implications for the water content of unmelted enstatite chondrites.

Several processes have been suggested to have then provided water to our planet later in its history. These include a late veneer of hydrated cometary material (Owen & Bar-Nun, 1995), and delivery via bombardment from outer-solar-system derived carbonaceous chondrite material (Alexander et al., 2012). These models imply that our planet's water budget – and by extension, its suitability for

life – is the result of the stochastic scattering of outer solar system material into the terrestrial planet forming region (Morbidelli et al., 2000). In this case, habitability would not be a natural consequence of Earth's formation from EC-like material.

Contrarily, recent measurements of the bulk compositions of ECs reveal they may unexpectedly contain high hydrogen concentrations (0.08 – 0.54 wt% H₂O)(Gray et al., 2022; Piani et al., 2020). Indeed, these measurements suggest ECs seemingly carry enough of this ingredient of water to account for up to ~14 times the mass of Earth's oceans. Moreover, isotopic measurements argue that Earth may have accreted as much as ~70 % of its volatile inventory, including hydrogen and nitrogen, from inner Solar System material (Martins et al., 2023; Piani et al., 2020; Savage et al., 2022; Steller et al., 2022). Later delivery of outer solar system material then likely contributed small amounts of volatile elements, which help to resolve the observed hydrogen and nitrogen isotopic ratios of Earth's surface (Alexander et al., 2012; Piani et al., 2020). Combined, these findings suggest that Earth, and other terrestrial planets, may have in fact formed with high initial inventories of hydrogen and other volatiles. However, one pivotal unknown in these recent measurements is the phase that carries ~80 % of the bulk hydrogen concentration in ECs. Without this information, we lack an understanding of the reason this element may be present in these meteorites in such high concentrations.

In all, current observations disagree as to whether ECs carry appreciable hydrogen. As such, it is unclear whether the proto-Earth contained abundant hydrogen from its inception or whether this element was predominantly delivered to our planet later in its history. It is therefore currently unknown whether Earth's water is a natural outcome of its formation from EC-like material. To constrain the amount of native hydrogen in ECs as well as explore the phase that may host this element in these meteorites, here we map an EC using micrometre-scale X-ray absorption near edge structure spectroscopy at the sulfur K edge (S-XANES).

Materials and Methods

We explored the speciation of S, and the abundance of different species of this element, in the EH3 chondrite LAR 12252 using micrometre-scale S-XANES at beamline I18 at the Diamond Light Source. We chose to study LAR 12252 due to its low weathering grade of A (NASA, 2022), which minimises the likelihood of widespread and/or prevalent terrestrial H-bearing weathering products.

We measured a 2D S-XANES map of an area of clastic matrix in this meteorite. This region included fragments of chondrules (which included mesostasis), enstatite grains, metal grains, various sulfide grains, and fine matrix (composed of an assortment of materials, all <5 μm). We measured these maps by sweeping an X-ray beam with a 5 μm spot size in 5 μm steps over an area 470 × 480 μm² large and measuring an S-XANES spectrum at each step (resulting in a total of 9,024 spectra). The energy of the beam was increased from 2465-2495 eV in 0.2 eV intervals at each individual spot, with an acquisition time of 0.05 s at each energy value. The mapped area was selected to minimise the number of large objects (≥100 μm) and visible signs of terrestrial weathering, such as rust. We also measured 15 spot spectra at points within mesostasis in 6 chondrules throughout our thin section, as well as in multiple cracks containing terrestrial weathering products. Chondrule mesostasis spots were selected following optical microscopy, ensuring that they represented the range of chondrule sizes and types present in the thin section.

To analyse our data, we fitted all our S-XANES spectra with multiple Gaussian peaks using IGOR Pro, discussed further in the SI. We chose this method over linear combination fitting due to the heterogeneities within the sample, absence of a complete reference database of spectra collected from meteorites, and the number of spectra collected. We chose to initially fit each spectrum only

between 2465-2478 eV (Fig. 1b) because this energy range contains the iron sulfide peak, the H-S peak, and parts of the S-edge step function and peaks due to S species at higher energies. We chose this approach because it allowed us to focus on the peaks of interest, making the fitting procedure more robust and straightforward (see SI). As seen in Figure 1, this method produced only small fitting errors. To determine the amplitude of the S^{6+} peak, we then simply fitted a single Gaussian curve in the energy range 2580-2590 eV. This approach means the recovered height of this peak is that above the background in this energy range, so it isolates the S^{6+} signal by not considering the S-edge step function or any other S species. To quantify the enrichment/depletion of hydrogen in the form of H-S in matrix compared to mesostasis, we normalised the amplitude of the H-S peak recovered from each point in our field of view to the average amplitude recovered from 15 spot spectra of chondrule mesostasis. To convert these ratios to an average hydrogen concentration, we calculated the average hydrogen enrichment factor in the fine matrix, and multiplied this by the average concentration of hydrogen in chondrule mesostasis (measured using secondary ion mass spectrometry) of 706 ppm (Piani et al., 2020; Thomassin et al., 2023; see SI).

Results

Peak Identification

The S-XANES spectra we collected display a variety of peaks, the presence of which depends principally on the phase that was measured (Figure 1a). S-XANES spectra of fine matrix and mesostasis typically contain four peaks (Figure 1a), providing evidence of sulphur in different compounds and oxidation states in these phases. By comparing peak energy and shape to reference spectra (Anzures et al., 2019; Lerner et al., 2021; Prange et al., 2002) as well as from the Database of Inorganic Sulfur Compounds from The European Synchrotron Radiation Facility, we can identify the species responsible for each peak.

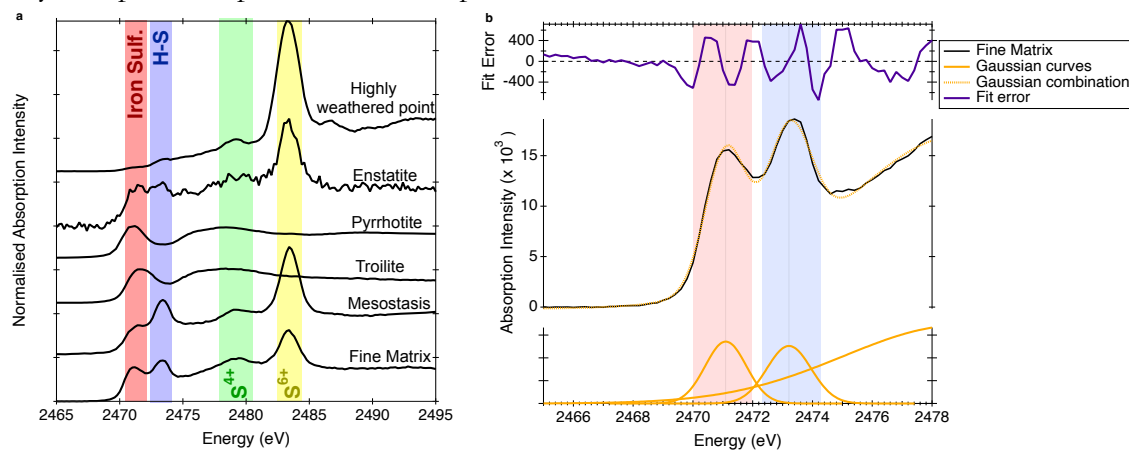


Figure 1a Representative S-XANES spectra measured in a variety of different phases in LAR 12252. Positions of peaks ascribed to species from reference spectra (Anzures et al., 2019; Lerner et al., 2021; Prange et al., 2002) are highlighted by vertical coloured bars. Spectra are normalised, so amplitudes here do not reflect sulfur content. Spectra from enstatite grains appear very noisy due to very low sulfur counts, and closely resemble spectra measured in metal grains. **1b** Peak fitting method used to extract the amplitudes of the iron sulfide and H-S peaks from the fine matrix spectra in 1a. We achieved this by creating a total fit (dashed orange in middle panel) from three Gaussian curves (orange, bottom panel) across the energy range 2468-2478 eV. This process yields small residual errors (purple, top panel). The highlighted peaks correspond to the same as in Figure 1a.

The peak at lowest energy, highlighted in red in Figure 1, is widespread in fine matrix and mesostasis and is ascribed to submicron-scale iron sulfides (troilite and pyrrhotite) (Anzures et al., 2019; Fleet, 2005; Klimm et al., 2012; Métrich et al., 2009). The energy of this peak varies from 2471.8 eV to 2471.2 eV, diagnostic of the composition of this mineral shifting from stoichiometric troilite to pyrrhotite ($Fe_{1-x}S$, $0 < x < 0.125$) (Head et al., 2018). Energies of all peak detected in our spectra are slightly (~ 1 eV) higher than reported in most previous studies (Anzures et al., 2019;

Fleet, 2005; Klimm et al., 2012; Métrich et al., 2009). Such variations are common in XANES studies and are attributed to differences in calibration of the monochromator (see SI).

Throughout the fine matrix and mesostasis, we also find a distinctive peak at ~ 2473.2 eV, highlighted in blue in Figure 1. Due to similar peak locations in reference spectra, this peak could be due to hydrogen bonded to S, native S, or pyrite (Bose et al., 2024). However, based on previously reported spectra (Bodeur & Esteva, 1985; Klimm et al., 2012; Orthous-Daunay et al., 2010; Prange et al., 2002), peak location relative to those of FeS and S^{6+} , and the absence of elemental S in previous sub-micron-scale compositional measurements (Lehner et al., 2014), we ascribe this peak to S bonded to H. Additionally, if this peak was caused by elemental S, rather than H-S, we would expect a broadening/shifting to higher energy of the wide absorption peak highlighted in green in Fig 1 than we observe. Our observation of H-S in chondrule mesostasis supports previous observations of hydrogen and the H-S bond in this phase (Thomassin et al., 2023). Additionally, our finding of the H-S peak throughout fine matrix demonstrates that H-S is a common form of hydrogen in ECs, and that this form of hydrogen is present in multiple phases.

In addition to reduced sulphides, many spectra also contain a peak at ~ 2483.4 eV corresponding to S^{6+} , the most oxidised form of sulfur, highlighted in yellow in figure 1. The amplitudes of these peaks vary widely among the points we measured, and they are at their highest in spot spectra collected within cracks where clear terrestrial weathering has occurred (Fig. S3). They also exist at much lower, but still variable, amplitudes in matrix and mesostasis. Different sulfates can be difficult to distinguish using S-XANES because different cations do not cause significant shifts in peak energy (Anzures et al., 2019). Despite this, we were able to identify $CaSO_4$ and $FeSO_4$ at some points in our mapped area of matrix, owing to minor peaks in the pre- and post-edge regions of the spectra (Anzures et al., 2019). The S^{6+} peak is absent within macroscopic ($>10 \mu m$) grains of metal, enstatite, and sulfides.

Additionally, we observe a small peak centred on ~ 2478 eV, shown in green in figure 1. The amplitude of this peak is affected by the presence of two species: a second wide absorption feature of troilite and pyrrhotite; and small amounts of S^{4+} likely formed through gradual photo-reduction of S^{6+} by the X-ray beam (Lerner et al., 2021; Wilke et al., 2008). We minimised the impact of photoreduction by mapping with as short acquisition times as possible.

Hydrogen Abundance

Because peak amplitude correlates with species abundance (Anzures et al., 2019; Fleet, 2005), we are able to estimate the concentrations of the different species in the matrix of LAR 12252 using S-XANES spectra. While the nature of complex geological samples like meteorites introduces specific challenges, we chose to estimate the concentration of H-S by comparing the amplitude of the peak at 2473.2 eV throughout our map to that of a phase with known hydrogen concentration, namely mesostasis. This chondrule glass has previously had its hydrogen concentration measured using background-corrected secondary ion mass spectrometry (Piani et al., 2020; Thomassin et al., 2023) (see SI). We measured 15 spot S-XANES spectra of chondrule mesostasis in LAR 12252, and used these to determine an average H-S peak amplitude for this phase (Fig. S8). We found our clastic matrix region contains H-S peak amplitudes that vary from ~ 0.1 -50 times average mesostasis (Figure 2b). The lowest relative amplitudes are found within the interiors of macroscale enstatite, metal, and sulfide grains. The highest amplitudes are in regions of fine matrix (see SI for our approach to identifying this phase). Adopting an average concentration of hydrogen in chondrule mesostasis of 706 ppm (Piani et al., 2020; Thomassin et al., 2023) and excluding points with extensive terrestrial weathering (in the form of large S^{6+} peaks, see *Discussion* section; Fig S5), we calculate that fine matrix in LAR 12252 contains an average of 6932 ± 2587 ppm H (2 standard error, taken from mesostasis H concentrations from (Piani et al., 2020; Thomassin et al., 2023; this

study). For a clastic matrix abundance of 9.6 wt% of the bulk meteorite (Lehner et al., 2014; Macke et al., 2010), and a fine matrix abundance of 50 wt% of the clastic matrix (Rubin et al., 2009), the fine matrix accounts for ~4.8 wt% of the bulk meteorite. This material therefore contributes an average of ~330 ppm hydrogen to the bulk concentration in EH3 chondrites. As such, it accounts for ~65 wt% of the total hydrogen budget (Piani et al., 2020).

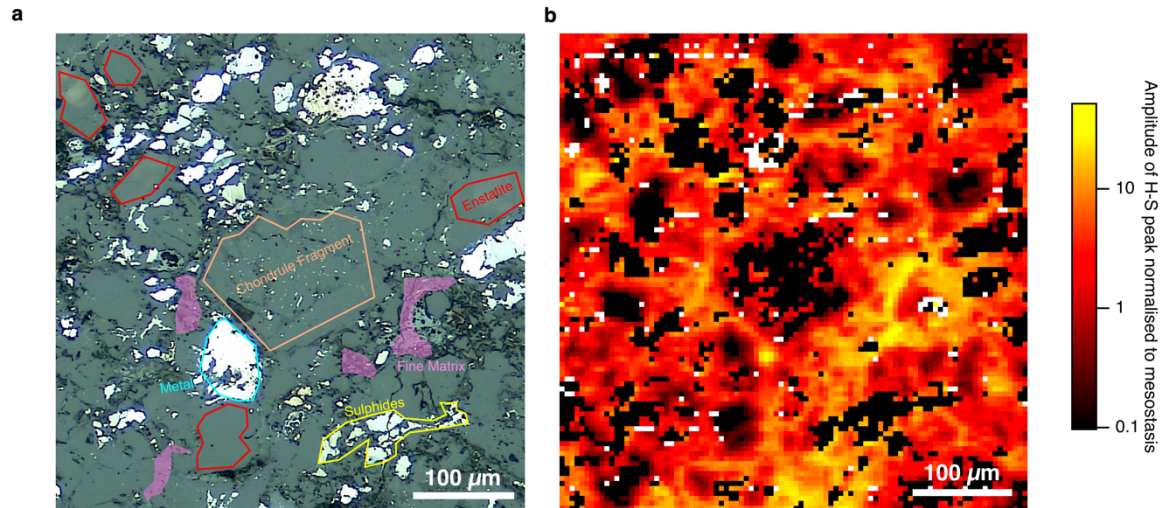


Figure 2a Optical image of the clastic matrix region in LAR 12252 that was studied using S-XANES. Notable phases include enstatite (examples outlined in red), sulphides (example outlined in yellow), a small chondrule fragment (outlined in orange), and fine matrix (examples highlighted in pink). **b** Corresponding map calculated from the S-XANES spectra of the region shown in **a**, showing the amplitude of the H-S peak at each point normalised to the average amplitude of point spectra measured from chondrule mesostasis (Fig. S8). Black pixels correspond to points where the S-XANES spectra that did not contain a resolvable H-S peak. White pixels correspond to points where the S-XANES spectra could not be fitted due to their quality or noise in the spectra.

Discussion

Is EC hydrogen native or a product of terrestrial weathering?

The primary difficulty with measuring the hydrogen content of a meteorite is ensuring that the hydrogen is not a product of terrestrial weathering. This is especially pertinent in ECs, where rare sulphide phases such as oldhamite react readily with atmospheric moisture to produce hydrated sulfates (Avril et al., 2021; Bland et al., 2006; Okada et al., 1981). While we avoided areas with extensive visible terrestrial weathering products, such as rust, much of the remaining meteorite could still have been modified by terrestrial weathering. Indeed, it has been suggested that previous measurements of bulk EC hydrogen concentrations were substantially influenced by the presence of terrestrial water/OH⁻ contained in weathering products (Gray et al., 2022; Peterson et al., 2023).

Figure 1 shows the presence of a peak at 2483.4 eV, attributed to the presence of oxidised, S⁶⁺-bearing species. However, the pre-terrestrial minerals observed petrographically in pristine ECs (including niningerite, oldhamite, and Si-bearing metal) argue these meteorites formed under particularly reducing conditions (Weisberg & Kimura, 2012) that will have led to the total absence of S⁶⁺-bearing minerals (Klimm et al., 2012). As such, the presence of S⁶⁺-bearing phases is most easily explained by terrestrial weathering, most likely of native sulfides. This is reinforced by spot spectra measured from a rust-bearing crack in the meteorite, which contained the highest S⁶⁺ peak amplitudes we measured (Fig. S3). Additionally, a grain of native troilite that has another crack running through it has been transformed into pyrrhotite via reactions with terrestrial water (Fig. S4). Crucially, these two crack spectra contain either no resolvable H-S peak at 2473.2 eV (the crack containing terrestrial pyrrhotite; Fig. S4) or one of very small amplitude relative to the S⁶⁺ peak (Fig. S3). Together, these observations strongly suggest that H-S is not a weathering product, so is instead native to EH3 meteorites.

Nonetheless, we chose to still filter the points we analysed to include only those that experienced the lowest extents of terrestrial weathering. We monitored this extent of weathering in each spectrum using the ratio of the amplitude of the S^{6+} peak to that of the FeS peak; as terrestrial weathering converted sulfide to sulfate (Bland et al., 2006) this ratio will have increased. This ratio varied widely throughout our mapped area, demonstrating that the local extent of terrestrial weathering was strongly heterogenous and was very low in some places (Fig. S6). To minimise the impact of weathering, we chose to only include spectra with an S^{6+} :FeS peak amplitude ratio <0.5 in our analysis, which we consider to be the most pristine (see SI).

Abundance of H

Our analysis demonstrates that H-S exists in fine matrix and mesostasis in ECs, and is in highest concentration in fine matrix. This phase accounts for $\sim 65\%$ of the bulk hydrogen value (Piani et al., 2020), arguing it is the dominant source of hydrogen in Earth's building blocks, capable of explaining ~ 9 times Earth's entire estimated present-day ocean water budget (Piani et al., 2020).

Previous studies have observed a relationship between S and H concentrations in mesostasis and have observed the S-H bond in this phase using Raman spectroscopy (Thomassin et al., 2023). Combined with our observation of the S-H bond in mesostasis and fine matrix from S-XANES, S-H appears to be the predominant carrier of hydrogen in EH3 chondrites, accounting for $\sim 80\%$ of their bulk budget (Fig. 3). Coupling our concentration estimate from fine matrix with previously measured concentrations of hydrogen in IOM (Piani et al., 2012), we can ascribe a source and carrier of $\sim 85\%$ of the bulk hydrogen budget of EH3 chondrites (Figure 3). Alongside our observation that this hydrogen is native, EH3 chondrites appear to carry larger concentrations of hydrogen than considered previously, supporting recent bulk compositional measurements (Piani et al., 2020).

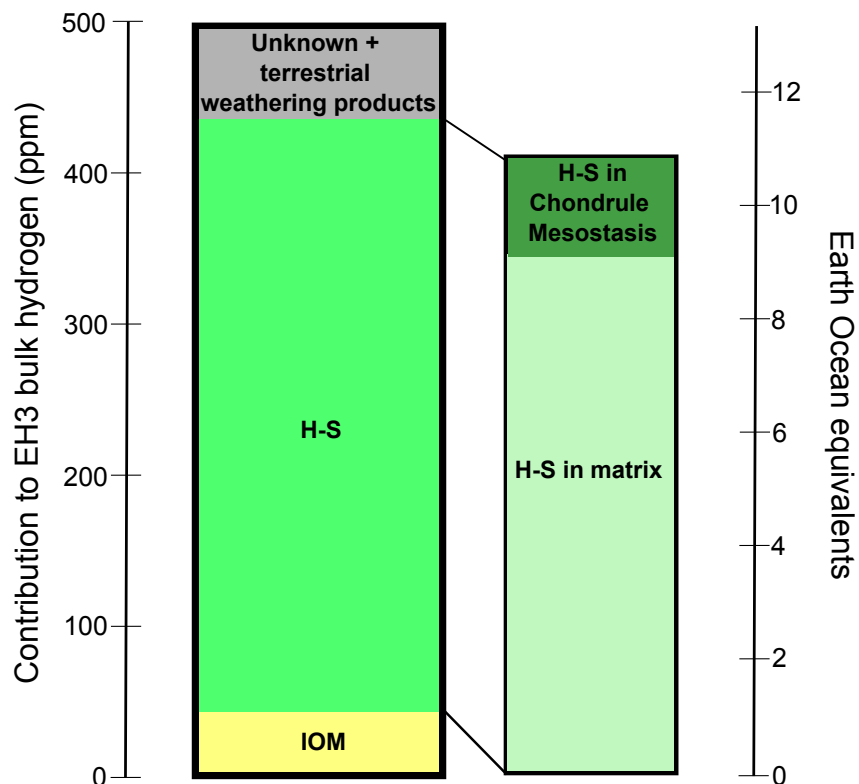


Figure 3 Relative contributions of different phases to the bulk EH3 hydrogen concentration (Piani et al., 2020). The concentration from IOM is taken from (Piani et al., 2012). The concentration in chondrule mesostasis is taken from (Piani et al., 2020; Thomassin et al., 2023). The concentration of H-S in matrix is from this study. We assume the unaccounted

proportion of hydrogen is associated with unexplored phases and terrestrial weathering products. Right hand axis shows the relative contributions in terms of their Earth ocean equivalent, based on the accretion of Earth by 100% EC-like material, where the mass of one ocean is 1.4×10^{21} kg (Piani et al., 2020).

Source of H

Despite appearing to host most of the hydrogen in ECs, the phase that carries the H-S bond we identified, and how it formed, were previously unknown. We found that spectra with large H-S peak amplitudes also exhibited large Fe-S peak amplitudes. In fact, the ratio of these two peak amplitudes varies between only $\sim 0 - 1$ (Figure 4) despite absolute amplitudes of these peaks, and relative amplitudes between other pairs of peaks, varying by several orders of magnitude throughout our mapped area (Fig. S2). This relationship suggests that the concentration of H-S is linked to the abundance of iron sulfides.

This variation in relative peak amplitudes can be used to further explore the origin of hydrogen in ECs. We found that spectra with a resolvable H-S peak (i.e., ratio of H-S peak amplitude to iron sulfide peak amplitude > 0) tend to contain an iron sulfide peak at lower energies than those that do not contain a resolvable H-S peak (Figure 4a). The energy of the iron sulfide peak reflects the stoichiometry of this phase, with the peak shifting the lower energy as the mineral become more iron deficient (i.e., as the mineralogy evolves from troilite to pyrrhotite (Head et al., 2018). This observation suggests that hydrogen is associated with pyrrhotite in ECs.

We can explore this in more detail by examining the relative peak amplitude of each individual spectrum. We find a trend between the energy position of each sulfide peak and the relative peak amplitude of the H-S peak (Figures 4b, S1). This relationship further indicates that the abundance of the H-S bond in the sulfide increases gradually as the sulfide loses Fe. Together, these observations argue that pyrrhotite is the source of H, which appears to substitute for Fe in the crystal structure.

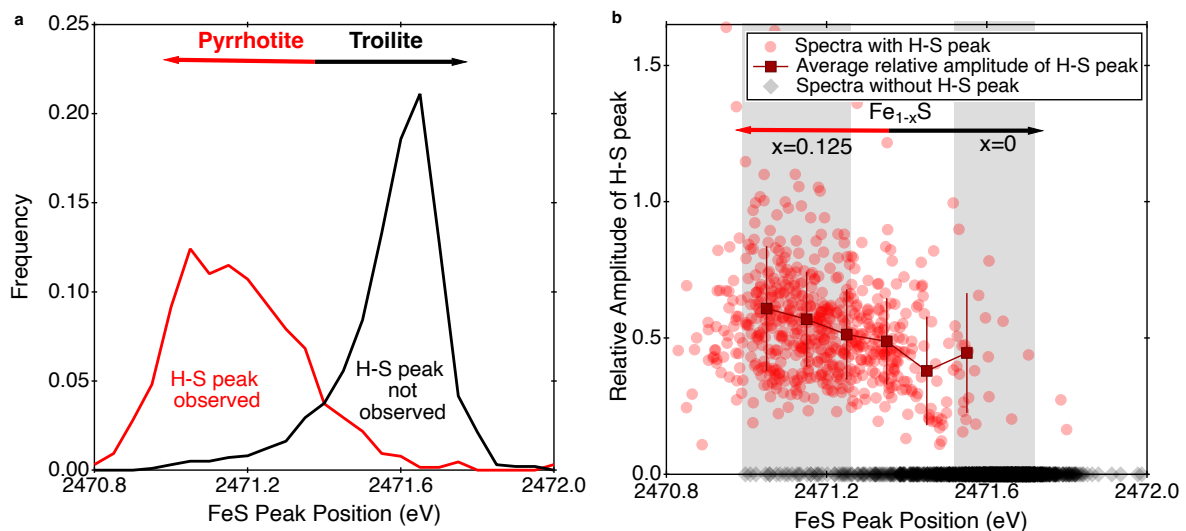


Figure 4a The distribution of the position of the FeS peak in analysed points throughout the mapped area for spectra with (red) and without (black) resolvable H-S peaks. Spectra with energies of the iron sulfide peak that indicate pyrrhotite is the dominant sulfide are more likely to carry the H-S peak, while spectra with iron sulfide peak energies consistent with troilite are less likely to display an H-S peak. **b** The amplitude of the H-S peak normalised to the amplitude of the corresponding FeS peak from each spectrum, plotted against the peak position of the FeS peak. Grey bars indicate the peak location of end member troilite and pyrrhotite. The transition between these bars represents a change in x in the pyrrhotite chemical formula, Fe_{1-x}S , $0 < x < 0.125$. Black diamonds on the horizontal axis represent spectra with no resolvable H-S peak. The dark red squares represent averages of the individual points in 0.1 eV-wide bands. The relative amplitude of the H-S peak increases as the abundance of pyrrhotite increases, further suggesting pyrrhotite is the carrier of hydrogen in ECs. The

slight increase at higher energy reflects the low number of points in this energy region containing an H-S peak, and difficulties identifying the H-S peak when its amplitude is small.

The presence of pyrrhotite is perhaps unexpected given the very reducing nebular environment in which ECs formed (Schrader et al., 2021; Weisberg & Kimura, 2012). Previous measurements of the concentrations of iron sulfides in ECs made using electron probe microanalysis find near-stoichiometric compositions in iron sulfides (Piani et al., 2016; Schrader et al., 2021). Our S-XANES spectra support this result, with the spectra from the centre of macroscopic ($\approx 10 \mu\text{m}$) iron sulfides matching reference spectra of troilite (Fig. 1a). However, in the fine matrix and approaching the edges of some macroscopic sulfide grains, the energy of the Fe-S peak shifts to lower values (Fig. S7). This shift argues that pyrrhotite exists as micron- to sub-micron-scale grains in fine matrix and micron- to sub-micron-scale rims on larger troilite grains. Although nebular troilite is more common, nebular pyrrhotite has been observed previously in multiple submicron settings: as rims $\sim 50 \text{ nm}$ wide coating larger grains of troilite in carbonaceous chondrites (Harries & Langenhorst, 2013); in the matrix of ECs as submicron grains (Lehner et al., 2014); and as $< 50 \text{ nm}$ grains in anhydrous interplanetary dust particles (Zolensky & Thomas, 1995). Combined with our results, these observations argue that iron sulphides exist as pyrrhotite when they are submicron in scale. This pyrrhotite has been proposed to have formed through low temperature sulfidation of pre-existing troilite in a high f_{S_2} environment in the disk (Harries & Langenhorst, 2013; Kerridge, 1976; Zolensky & Thomas, 1995), or alternatively through the sulfidation of Fe metal by H_2S (Gainsforth et al., 2017). Our results suggest this former process occurred only on the outer part (perhaps $< 1 \mu\text{m}$) of troilite grains, which would cause an entire troilite grain to transform to pyrrhotite if it was below this critical size. Our S-XANES data suggest that H_2 from the disk also reacted into the pyrrhotite structure, perhaps into the Fe vacancy, during this low-temperature sulfidation of troilite. This process enabled high concentrations of hydrogen to be locked into this phase in ECs. Matrix in these meteorites therefore has the ideal mineralogy (i.e., abundant sub-micron sulfides; (Lehner et al., 2014) and formation environment (i.e., an S_2 -rich and H_2 -rich gas) to store appreciable hydrogen in the form H-S bonds in pyrrhotite.

Our spectra from mesostasis indicate that submicron sulfides also exist in this glass. As such, it is plausible that the hydrogen in mesostasis is also hosted in grains of pyrrhotite, as in the fine matrix. In this case, the carrier phase of hydrogen in both mesostasis and matrix would be the same, so we chose not to apply a correction for the phase that carries hydrogen when calculating the hydrogen concentrations from mesostasis values.

Implications

In conventional models of the origin of volatile elements on Earth, water was the result of a stochastic, late bombardment of carbonaceous material onto our planet (Alexander et al., 2012). This scenario is capable of explaining Earth's water budget, but means that water and habitable conditions on Earth are a result of a chance scenario. The combined D and ^{15}N compositions of the oceans and atmosphere compared to the mantle (Piani et al., 2020) indicate that there is a contribution from this carbonaceous source, at least on the surface of our planet. However, the D and ^{15}N isotopic composition of the mantle indicate that this bombardment struggles to explain the bulk of the hydrogen within our planet (Piani et al., 2020). As such, volatiles delivered by bombardment likely correspond to a small proportion of the total budget throughout Earth.

Our findings suggest that pristine ECs contain enough hydrogen to explain the entire water budget of our planet, requiring that less water needs to have been delivered to Earth after it formed. In this scenario, ECs seemingly became enriched in hydrogen through sulfidation of troilite in an S_2 -rich and H_2 -rich nebular gas. As such, the water budget of Earth is not the result of a chance bombardment. Instead, it can be a natural and determined consequence of the formation of EC-like material in the hot, reducing, and sulfidising environment of the inner solar system.

Additionally, this means that other terrestrial planets that have been proposed to have formed from similar material – including Mars (Brasser et al., 2018), Mercury (Namur et al., 2016), and perhaps Venus – may have had similar early volatile budgets to the proto-Earth. A key question now is the hydrogen content of metamorphosed ECs (e.g., EH4-EH6) and aubrites, as well as the proportions of each of these types of meteorites in the proto-Earth.

Acknowledgements

The authors would like to thank Diamond Light Source for beamtimes (proposals SP31591-1 and SP35606), and staff of beamline I18 for assistance with data collection. The authors would also like to thank the Antarctic Search for Meteorites (ANSMET) program (which has been funded by NSF and NASA and curated by the Department of Mineral Sciences of the Smithsonian Institution and Astromaterials Curation Office at NASA Johnson Space Center) for use of their meteorite samples. JFJB acknowledges funding through UKRI grant number EP/Y014375/1. TJB acknowledges funding through STFC.

References

- Alexander, C. M. O., Bowden, B., Fogel, F., Howard, H., Herd, H., & Nittler, N. (2012). The Provenances of Asteroids, and Their Contributions to the Volatile Inventories of the Terrestrial Planets. *Science*, *337*(6095), 721–723. <https://doi.org/10.1126/science.1223474>
- Anzures, B., Parman, S., Milliken, R., Lanzirrotti, A., & Newville, M. (2019). XANES Spectroscopy of Sulfides Stable under Reducing Conditions. *American Mineralogist*. <https://doi.org/10.2138/am-2020-7146>
- Avril, C., Malavergne, V., van Hullebusch, E. D., Brunet, F., Borensztajn, S., Labanowski, J., Hennem, L., & Guyot, F. (2021). Aqueous alteration and bioalteration of a synthetic enstatite chondrite. *Meteoritics and Planetary Science*, *56*(3), 601–618. <https://doi.org/10.1111/maps.13641>
- Bland, P. A., Zolensky, M. E., Benedix, G. K., & Sephton, M. A. (2006). *Weathering of Chondritic Meteorites* (p. 853). <https://ui.adsabs.harvard.edu/abs/2006mess.book..853B>
- Bodeur, S., & Esteva, J. M. (1985). Photoabsorption spectra of H₂S, CH₃SH and SO₂ near the sulfur K edge. *Chemical Physics*, *100*(3), 415–427. [https://doi.org/10.1016/0301-0104\(85\)87067-1](https://doi.org/10.1016/0301-0104(85)87067-1)

- Bose, M., Root, R. A., Guan, Y., Eaton, J., Wittmann, A., Skrmetti, T., & Desch, S. J. (2024). Evidence of both molecular cloud and fluid chemistry in Ryugu regolith. *Science Advances*, *10*(30), eadp3037. <https://doi.org/10.1126/sciadv.adp3037>
- Brasser, R., Dauphas, N., & Mojzsis, S. J. (2018). Jupiter's Influence on the Building Blocks of Mars and Earth. *Geophysical Research Letters*, *45*(12), 5908–5917. <https://doi.org/10.1029/2018GL078011>
- Dauphas, N. (2017). The isotopic nature of the Earth's accreting material through time. *Nature*, *541*(7638), 521–524. <https://doi.org/10.1038/nature20830>
- Fleet, M. E. (2005). XANES SPECTROSCOPY OF SULFUR IN EARTH MATERIALS. *The Canadian Mineralogist*, *43*(6), 1811–1838. <https://doi.org/10.2113/gscanmin.43.6.1811>
- Gainsforth, Z., Lauretta, D. S., Tamura, N., Westphal, A. J., Jilly-Rehak, C. E., & Butterworth, A. L. (2017). Insights into solar nebula formation of pyrrhotite from nanoscale disequilibrium phases produced by H₂S sulfidation of Fe metal. *American Mineralogist*, *102*(9), 1881–1893. <https://doi.org/10.2138/am-2017-5848>
- Gray, M. L., Weisberg, M. K., Alexander, C. M. O., Wang, J., & Ebel, D. S. (2022). H₂O Abundances of an EH6 Chondrite and Potential Implications for Earth. *2695*, 6452. <https://ui.adsabs.harvard.edu/abs/2022LPICo2695.6452G>
- Harries, D., & Langenhorst, F. (2013). The nanoscale mineralogy of Fe,Ni sulfides in pristine and metamorphosed CM and CM/CI-like chondrites: Tapping a petrogenetic record. *Meteoritics & Planetary Science*, *48*(5), 879–903. <https://doi.org/10.1111/maps.12089>
- Head, E., Lanzirotti, A., Newville, M., & Sutton, S. (2018). Vanadium, sulfur, and iron valences in melt inclusions as a window into magmatic processes: A case study at Nyamuragira volcano, Africa. *Geochimica et Cosmochimica Acta*, *226*, 149–173. <https://doi.org/10.1016/j.gca.2018.01.033>
- Javoy, M., Kaminski, E., Guyot, F., Andrault, D., Sanloup, C., Moreira, M., Labrosse, S., Jambon, A., Agrinier, P., Davaille, A., & Jaupart, C. (2010). The chemical composition of the

- Earth: Enstatite chondrite models. *Earth and Planetary Science Letters*, 293(3), 259–268.
<https://doi.org/10.1016/j.epsl.2010.02.033>
- Kerridge, J. F. (1976). Formation of iron sulphide in solar nebula. *Nature*, 259(5540), Article 5540. <https://doi.org/10.1038/259189a0>
- Klimm, K., Kohn, S. C., & Botcharnikov, R. E. (2012). The dissolution mechanism of sulphur in hydrous silicate melts. II: Solubility and speciation of sulphur in hydrous silicate melts as a function of fO₂. *Chemical Geology*, 322–323, 250–267.
<https://doi.org/10.1016/j.chemgeo.2012.04.028>
- Lehner, S. W., McDonough, W. F., & Németh, P. (2014). EH3 matrix mineralogy with major and trace element composition compared to chondrules. *Meteoritics & Planetary Science*, 49(12), 2219–2240. <https://doi.org/10.1111/maps.12391>
- Lerner, A. H., Muth, M. J., Wallace, P. J., Lanzirotti, A., Newville, M., Gaetani, G. A., Chowdhury, P., & Dasgupta, R. (2021). Improving the reliability of Fe- and S-XANES measurements in silicate glasses: Correcting beam damage and identifying Fe-oxide nanolites in hydrous and anhydrous melt inclusions. *Chemical Geology*, 586, 120610.
<https://doi.org/10.1016/j.chemgeo.2021.120610>
- Macke, R. J., Consolmagno, G. J., BRITT, D. T., & HUTSON, M. L. (2010). Enstatite chondrite density, magnetic susceptibility, and porosity. *Meteoritics & Planetary Science*, 45(9), 1513–1526. <https://doi.org/10.1111/j.1945-5100.2010.01129.x>
- Martins, R., Kuthning, S., Coles, B. J., Kreissig, K., & Rehkämper, M. (2023). Nucleosynthetic isotope anomalies of zinc in meteorites constrain the origin of Earth's volatiles. *Science (New York, N.Y.)*, 379(6630), 369–372. <https://doi.org/10.1126/science.abn1021>
- Marty, B. (2012). The origins and concentrations of water, carbon, nitrogen and noble gases on Earth. *Earth and Planetary Science Letters*, 313–314, 56–66.
<https://doi.org/10.1016/j.epsl.2011.10.040>

- Métrich, N., Berry, A. J., O'Neill, H. St. C., & Susini, J. (2009). The oxidation state of sulfur in synthetic and natural glasses determined by X-ray absorption spectroscopy. *Geochimica et Cosmochimica Acta*, 73(8), 2382–2399. <https://doi.org/10.1016/j.gca.2009.01.025>
- Morbidelli, A., Chambers, J., Lunine, J. I., Petit, J. M., Robert, F., Valsecchi, G. B., & Cyr, K. E. (2000). Source regions and timescales for the delivery of water to the Earth. *Meteoritics & Planetary Science*, 35(6), 1309–1320. <https://doi.org/10.1111/j.1945-5100.2000.tb01518.x>
- Namur, O., Collinet, M., Charlier, B., Grove, T. L., Holtz, F., & McCammon, C. (2016). Melting processes and mantle sources of lavas on Mercury. *Earth and Planetary Science Letters*, 439, 117–128. <https://doi.org/10.1016/j.epsl.2016.01.030>
- NASA. (2022). *Antarctic Meteorite Petrographic Description* (Vol. 2023, Issue 12th April). <https://curator.jsc.nasa.gov/antmet/samples/petdes.cfm?sample=LAR12252>
- Okada, A., Keil, K., & Taylor, G. J. (1981). UNUSUAL WEATHERING PRODUCTS OF OLDHAMITE PARENTAGE IN THE NORTON COUNTY ENSTATITE ACHONDRITE. *Meteoritics*, 16(2), 141–152. <https://doi.org/10.1111/j.1945-5100.1981.tb00539.x>
- Orthous-Daunay, F.-R., Quirico, E., Lemelle, L., Beck, P., deAndrade, V., Simionovici, A., & Derenne, S. (2010). Speciation of sulfur in the insoluble organic matter from carbonaceous chondrites by XANES spectroscopy. *Earth and Planetary Science Letters*, 300(3), 321–328. <https://doi.org/10.1016/j.epsl.2010.10.012>
- Owen, T., & Bar-Nun, A. (1995). Comets, Impacts, and Atmospheres. *Icarus*, 116(2), 215–226. <https://doi.org/10.1006/icar.1995.1122>
- Peterson, L. D., Newcombe, M. E., Alexander, C. M. O., Wang, J., Klein, F., Bekaert, D. V., & Nielsen, S. G. (2023). The H content of aubrites: An evaluation of bulk versus in situ methods for quantifying water in meteorites. *Earth and Planetary Science Letters*, 620, 118341. <https://doi.org/10.1016/j.epsl.2023.118341>

- Piani, L., Marrocchi, Y., Libourel, G., & Tissandier, L. (2016). Magmatic sulfides in the porphyritic chondrules of EH enstatite chondrites. *Geochimica et Cosmochimica Acta*, *195*, 84–99. <https://doi.org/10.1016/j.gca.2016.09.010>
- Piani, L., Marrocchi, Y., Rigaudier, T., Vacher, L., Thomassin, D., & Marty, B. (2020). Earth's water may have been inherited from material similar to enstatite chondrite meteorites. *Science*, *369*(6507), 1110–1113. <https://doi.org/10.1126/science.aba1948>
- Piani, L., ROBERT, F., BEYSSAC, O., BINET, L., BOUROT-DENISE, M., DERENNE, S., GUILLOU, C. L., MARROCCHI, Y., MOSTEFAOUI, S., ROUZAUD, J.-N., & THOMEN, A. (2012). Structure, composition, and location of organic matter in the enstatite chondrite Sahara 97096 (EH3). *Meteoritics & Planetary Science*, *47*(1), 8–29. <https://doi.org/10.1111/j.1945-5100.2011.01306.x>
- Prange, A., Dahl, C., Trüper, H. G., Behnke, M., Hahn, J., Modrow, H., & Hormes, J. (2002). Investigation of S-H bonds in biologically important compounds by sulfur K-edge X-ray absorption spectroscopy. *The European Physical Journal D - Atomic, Molecular, Optical and Plasma Physics*, *20*(3), 589–596. <https://doi.org/10.1140/epjd/e2002-00156-5>
- Rubin, A. E., Griset, C. D., CHOI, B.-G., & WASSON, J. T. (2009). Clastic matrix in EH3 chondrites. *Meteoritics & Planetary Science*, *44*(4), 589–601. <https://doi.org/10.1111/j.1945-5100.2009.tb00754.x>
- Savage, P. S., Moynier, F., & Boyet, M. (2022). Zinc isotope anomalies in primitive meteorites identify the outer solar system as an important source of Earth's volatile inventory. *Icarus*, *386*, 115172. <https://doi.org/10.1016/j.icarus.2022.115172>
- Schrader, D. L., Davidson, J., McCoy, T. J., Zega, T. J., Russell, S. S., Domanik, K. J., & King, A. J. (2021). The Fe/S ratio of pyrrhotite group sulfides in chondrites: An indicator of oxidation and implications for return samples from asteroids Ryugu and Bennu. *Geochimica et Cosmochimica Acta*, *303*, 66–91. <https://doi.org/10.1016/j.gca.2021.03.019>

- Steller, T., Burkhardt, C., Yang, C., & Kleine, T. (2022). Nucleosynthetic zinc isotope anomalies reveal a dual origin of terrestrial volatiles. *Icarus*, *386*, 115171.
<https://doi.org/10.1016/j.icarus.2022.115171>
- Thomassin, D., Piani, L., Villeneuve, J., Caumon, M.-C., Bouden, N., & Marrocchi, Y. (2023). The high-temperature origin of hydrogen in enstatite chondrite chondrules and implications for the origin of terrestrial water. *Earth and Planetary Science Letters*, *616*, 118225. <https://doi.org/10.1016/j.epsl.2023.118225>
- Weisberg, M. K., & Kimura, M. (2012). The unequilibrated enstatite chondrites. *Geochemistry*, *72*(2), 101–115. <https://doi.org/10.1016/j.chemer.2012.04.003>
- Wilke, M., Jugo, P. J., Klimm, K., Susini, J., Botcharnikov, R., Kohn, S. C., & Janousch, M. (2008). The origin of S⁴⁺ detected in silicate glasses by XANES. *American Mineralogist*, *93*(1), 235–240. <https://doi.org/10.2138/am.2008.2765>
- Zolensky, M. E., & Thomas, K. L. (1995). Iron and iron-nickel sulfides in chondritic interplanetary dust particles. *Geochimica et Cosmochimica Acta*, *59*(22), 4707–4712.
[https://doi.org/10.1016/0016-7037\(95\)00329-0](https://doi.org/10.1016/0016-7037(95)00329-0)

The Source of Hydrogen in Earth's Building Blocks - Supporting Information

Thomas J. Barrett¹, James F.J. Bryson¹, Kalotina Geraki²

1. Department of Earth Sciences, University of Oxford, Oxford, OX1 3AN, UK.
2. Diamond Light Source, Harwell Science and Innovation Campus, Didcot, OX11 0DE, UK.

Email: thomas.barrett@st-annes.ox.ac.uk

Methods

Gaussian Peak Fitting

The energy and shape of a peak in an S-XANES spectrum is controlled by: the redox state of sulfur; the cation; the bond character; and the local bonding environment (Anzures et al., 2019). Unlike more oxidised sulfur compounds, sulfides (S²⁻) with differing cations display characteristic spectra with peaks at specific energies and with distinct shapes (Fleet, 2005). As such, species such as H-S produce a characteristic peak within an S-XANES spectrum. The amplitude of an absorption peak is proportional to species abundance (Fleet, 2005), allowing quantitative estimates of the concentrations of different sulfur species within complex geological samples, such as meteorites, to be recovered.

In order to extract peak amplitudes corresponding to iron sulfide and H-S in LAR 12252, we fitted 3 Gaussian curves simultaneously across the energy range 2468 – 2478 eV in all 9,024 of our spectra. The first 2 Gaussians have approximately equal width (~1 eV) and were fit to FeS at 2471.2 – 2471.8 eV (depending on stoichiometry) and H-S at ~2473.2 eV. A third curve of larger width (~4-5 eV) was fit around 2478 eV, which captures both the second absorption peak of FeS and the step at the S K edge. Although a Gaussian only approximates the shape of this wider feature, we do not use any of the properties of this peak in our analysis, so the quality of fit in this part of the spectra is less crucial. This three-peak approach produced very small fitting errors against the measured spectrum (Fig. 1b in the main text) around the energies of the FeS and H-S peaks (i.e., the key peaks of interest). Gaussian curves fitted to FeS and H-S peaks were constrained by energy (eV) boundaries 2470.8 <FeS<2472 and 2472<H-S<2474, as well as maximum (1.5 eV) and minimum (0 eV) widths, to ensure that fitting was consistent and accurate between different spectra. Certain fits were manually rejected and excluded from calculations where it was obvious that the spectra contained high noise levels or spurious data (white points in Fig. 2b in the main text). High noise levels were most common in spectra with very low sulfur counts (e.g., in the interiors of macroscale metal or enstatite grains).

Differences in monochromator calibration meant that our peaks were not in the locations typically stated in the literature. However, we were able to assign some peaks with certainty by measuring spot spectra in large phases (on the scale of hundreds of micrometres to millimetres) that we could identify using light microscopy. For instance, we were able to unambiguously assign spectra in our region of interest to troilite using this approach (e.g., Fig S4). This led us to identify that all peaks in our data are shifted by very similar energies (~1 eV), compared to literature data, including the database for inorganic sulfur compounds from The European Synchrotron Radiation Facility. This shift allowed us to confidently ascribe the peak we find at ~2473.2 eV to either H-S or elemental sulfur, which are challenging to distinguish due to very similar peak locations (Bose et al., 2024). However, as discussed in the main text, the absence of elemental S in previous micro- and nano-analytical studies e.g. (Lehner et al., 2014; Weisberg & Kimura, 2012) allows us to confidently ascribe this peak to H-S.

H concentration calculation

In order to calculate the contribution of H-S to the total EC hydrogen budget, we compare the amplitude of the H-S peak in fine matrix to a phase with known H concentrations – chondrule mesostasis – under the assumption that all H in mesostasis is in the form H-S. The H concentration of mesostasis in EH3 chondrites has been measured (Piani et al., 2020; Thomassin et al., 2023) several times (n_1) across 14 chondrules using background-corrected secondary ion mass spectroscopy, with an average concentration of 706 ppm H, ($\bar{C}_{H \text{ Mesostasis (SIMS)}}$).

$$\bar{C}_{H \text{ Mesostasis (SIMS)}} = \frac{\sum \text{SIMS Measurements}}{n_1}$$

We measured S-XANES spot spectra at 15 (n_2) individual points within chondrule mesostasis (Fig. S8). We recovered the amplitude of the H-S peak from each of these spectra using our multi-peak fitting method, and calculated the average amplitude, $\overline{Amp}_{Mesostasis}$.

$$\overline{Amp}_{Mesostasis} = \frac{\sum Mesostasis\ peak\ amplitudes}{n_2}$$

We then calculated the abundance of H-S at each point throughout our region of matrix relative to mesostasis by normalizing the H-S peak amplitude from each individual point by $\overline{Amp}_{Mesostasis}$.

We identified points in our region of interest that are fine matrix using a series of peak amplitude ratios. Firstly, we exclude all points with H-S/FeS peak amplitude ratios either equal to 0 or greater than 2. The first of these criteria ensures that points in large ($>5\ \mu\text{m}$) grains of metal, enstatite, and sulfide (i.e., with no detectable H-S peak) are not included in the analysis. The second of these criteria ensures that we do not include points that have artificially low amounts of iron sulfide due to terrestrial weather (see *Weathering* section). Our final step is to consider the amplitude of the H-S peak relative to that found across the range of spectra measured in mesostasis (Fig. S8). By qualitatively assessing our S-XANES map alongside optical microscopy images (Fig. 2 in the main text), we find that fine matrix displays H-S peak amplitudes that are routinely higher than that of mesostasis, reflecting the higher concentration of hydrogen in fine matrix. Therefore, we chose to isolate fine matrix by analysing only points with H-S peak amplitude greater than the range of values measured throughout chondrule mesostasis (Fig S8). Our intention is that all these steps led to only fine matrix being included in our analysis.

We then calculated an average, representative hydrogen concentration for fine matrix in the mapped area, $H\ conc$, by multiplying the relative peak amplitude by the average mesostasis hydrogen concentration, and dividing the sum by the number of points in the analysis (n_3).

$$H\ conc = \frac{\sum \left(\frac{Point\ Peak\ Amp}{\overline{Amp}_{Mesostasis}} \times \overline{C}_H\ Mesostasis\ (SIMS) \right)}{n_3}$$

Weathering

Enstatite chondrites are particularly susceptible to weathering on Earth. As discussed in the main text, the detection of an S^{6+} peak in our spectra demonstrates the presence of some terrestrial alteration products throughout our region of interest. The total absence or small relative amplitude of H-S peaks in spectra collected from cracks argues the H-S peak is not created by weathering, and is instead native to the enstatite chondrites. In the case of the rust-bearing crack with a particularly large S^{6+} peak (Fig. S3), we believe that the H-S peak is due to native H that was present before weathering. This because the size of the H-S peak does not scale with the size of the S^{6+} peak. Nonetheless, we chose to exclude points in our analysis that contained evidence of more extensive terrestrial weathering. FeS is thought to react during terrestrial weathering to produce sulphates (Bland et al., 2006). As such, we chose to limit the spectra we analyzed to those with a low S^{6+}/FeS peak amplitude ratio of <0.5 . This threshold ensured regions of the meteorite that experienced more extensive terrestrial weathering were excluded from our analysis, so we are as confident as possible that we are targeting only the most pristine points that may contain pre-terrestrial hydrogen. As discussed in the previous section, we also excluded points with H-S/FeS peak amplitude ratios greater than 2 because this large value could reflect the reduction of iron sulfides due to terrestrial weathering.

Notably, when points with higher ratios of S^{6+}/FeS peak amplitude were included in our analysis, the average relative H-S amplitude decreased. This trend suggests that weathering reactions may actually have decreased the amount of hydrogen stored as H-S. This is consistent with our proposal that H-S is stored of grains of pyrrhotite, because weathering would act to remove the host phase of H-S through destruction of this mineral, rather than introducing H.

Sources of error

Because the total bulk H content is calculated using previously measured H concentrations in mesostasis ($\overline{C}_H\ Mesostasis\ (SIMS)$) (Piani et al., 2020; Thomassin et al., 2023), possible errors in these

literature data derived from their SIMS measurements, as well as elsewhere in their methods, will carry through to the value calculated in this study.

In this study, we choose the dominant source of uncertainty in our total hydrogen concentration to be that due to the range of hydrogen concentrations measured in chondrule mesostasis, in both our work (i.e., the spread of H-S peak amplitudes measured among chondrule mesostasis, Fig. S8) and previous studies (i.e., the range of measured H concentrations in mesostasis; Piani et al., 2020; Thomassin et al., 2023). We chose this because it produces the largest value of uncertainty, and so is the most conservative approach. This approach produced a 2 standard error value of 2587 ppm on the average H concentration that we calculated (i.e., ~37% of our average H concentration).

We note that there are additional sources of error. One comes from difficulties in defining clastic matrix and fine matrix, which have varied definitions in the literature (Lehner et al., 2014; Macke et al., 2010; Rubin et al., 2009). We minimised this error by targeting an area with few large clasts, and averaging matrix volumes previously reported in the literature (Lehner et al., 2014; Macke et al., 2010; Rubin et al., 2009).

Additionally, there is potential for error in our quantification derived from the compositional difference between matrix and mesostasis. Atomic arrangement and phase type can influence peak intensity and shape due to various multiple-scattering effects, which can be dealt with using phase correction. However, based on our observation of sub-micron scale sulfides in mesostasis (i.e., a consistent FeS peak), as well as the H-S/FeS peak amplitude ratio being similar between mesostasis and matrix, we propose that the carrier of H-S could be sulfide grains in both the mesostasis and fine matrix. As such, we chose not to apply a correction to account for differences in phases studied.

Finally, there are inevitable sources of analytical error in other aspects of the analysis, such as noise in our spectra and fitting peaks to these data. However, our adopted multi-peak fitting approach produced only small residual errors (Fig. 1b), typically limited to around 1% of the peak absorption intensity. As such, we consider these sources of error as relatively minor.

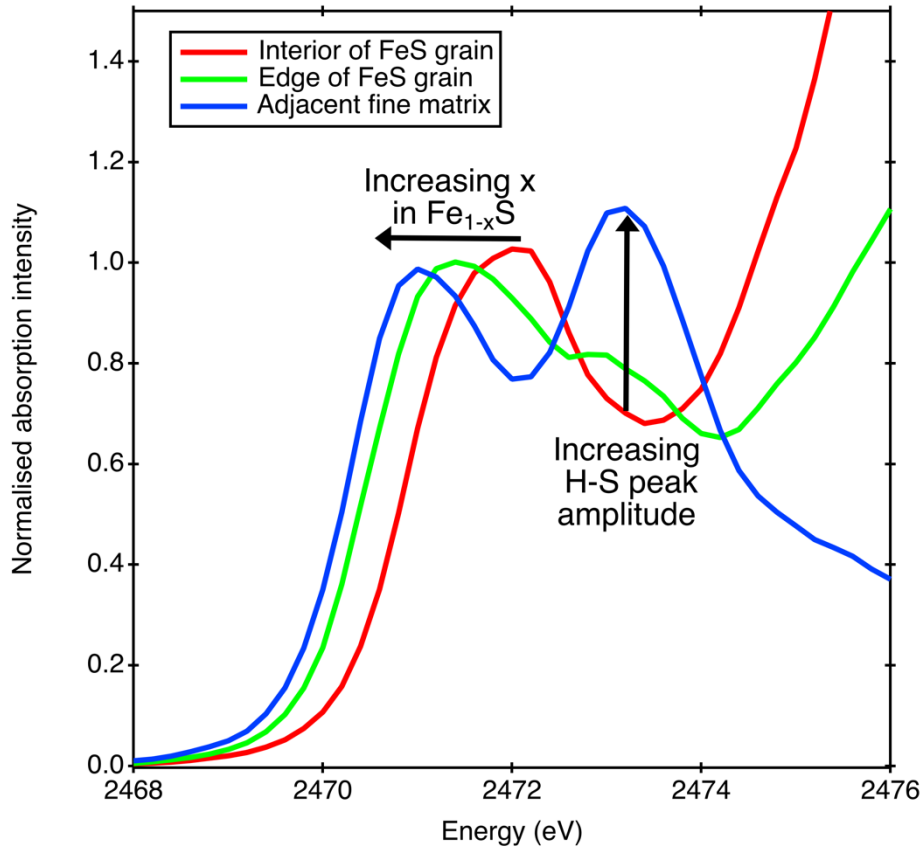


Fig. S2. XANES spectra with amplitudes normalized at the FeS peak. The red spectrum is taken from the interior of a grain of troilite (FeS). The green spectrum is taken from the edge of that FeS grain. The blue spectrum is from the fine matrix just outside of this FeS grain. As the spectra move from the interior of a macroscale sulfide to the fine matrix, the position of the iron sulfide peak shifts the lower energy and the relative amplitude of the H-S peak increases. The lateral shift in FeS peak position is indicative of the increase in x in Fe_{1-x}S , moving from troilite to pyrrhotite. Together, these trends argue that H is found in grains of pyrrhotite.

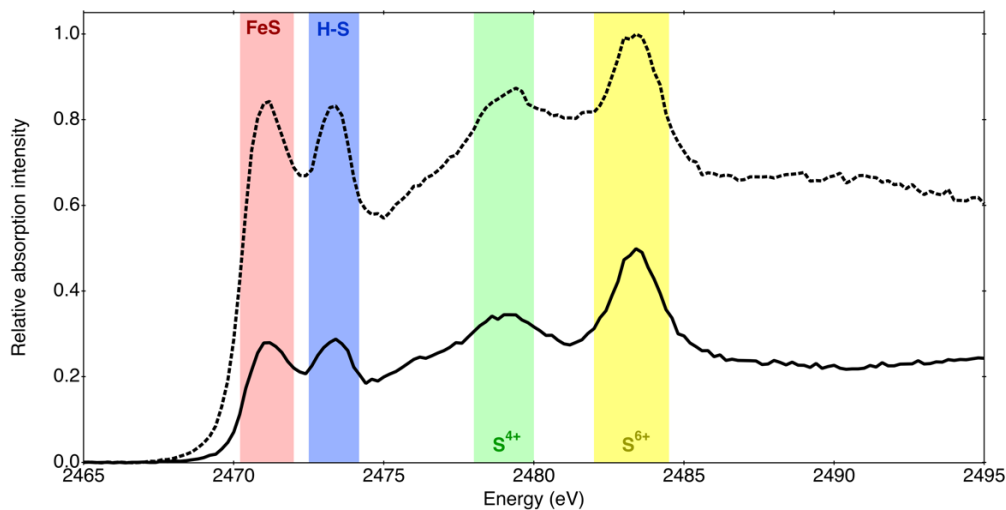


Fig. S2. Two spectra from matrix points in LAR 12252, marked by the solid and dashed lines, both normalized to maximum absorption intensity (i.e., at ~ 2483 eV) in the dashed curve. The ratio between FeS and H-S peak amplitude is similar in these spectra, and others throughout the matrix, demonstrating that H-S concentration is tied to the abundance of iron sulfides. Notably, the absolute amplitude of the peaks varies greatly throughout different areas of matrix in the meteorite, demonstrating the heterogeneity in H-S and iron sulfide abundance.

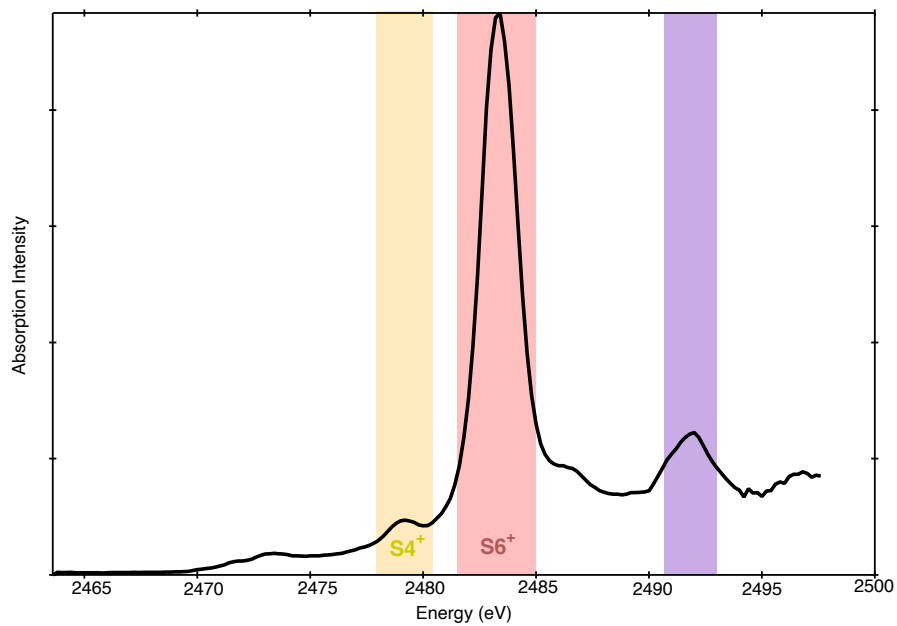


Fig. S3. XANES spot spectrum collected from a rust-bearing crack in LAR 12252. The high amplitude peak at ~2483 eV corresponds to the presence of S^{6+} -bearing species, which is a terrestrial weathering product. The spectrum contains a peak at 2473.2 eV, though its amplitude is very small relative to the S^{6+} peak, suggesting that H-S is not a weathering product, but instead a small amount of native H-S that survived terrestrial weathering. The purple band corresponds to a secondary absorption peak produced by the sulfate species present here, likely $CaSO_4$ based on spectra from the database for inorganic sulfur compounds from The European Synchrotron Radiation Facility.

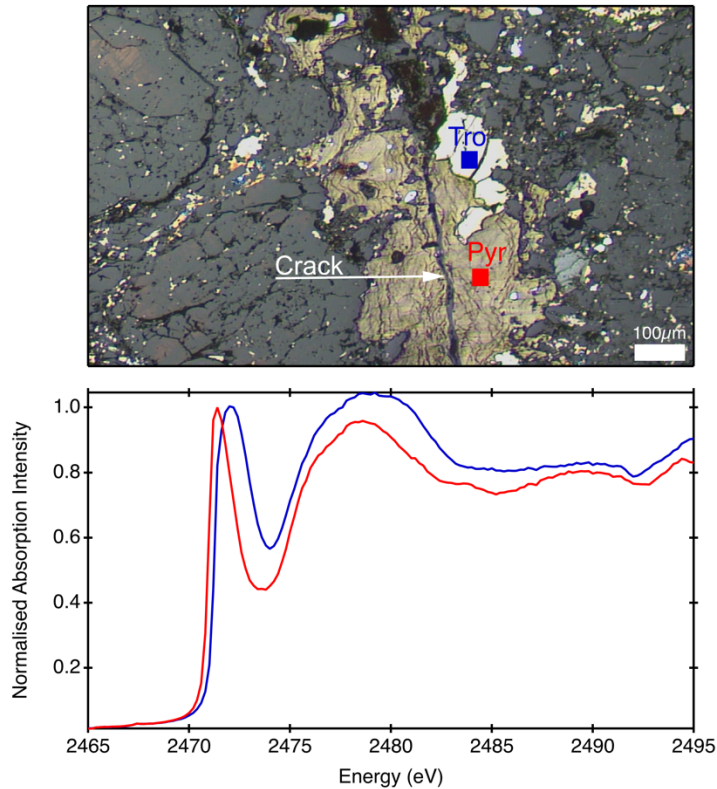


Fig. S4. XANES spectra collected from two points within a terrestrially altered crack within the meteorite, with their amplitudes normalized at the initial FeS absorption peak at 2471.2 - 2471.8eV, depending on the stoichiometry. The blue square represents the spot where the blue spectrum was collected, which is a grain of stoichiometric FeS (troilite). The red square is the location where the spectrum in red was collected, which is a grain of pyrrhotite. The pyrrhotite here clearly follows the crack, arguing that it is formed by terrestrial weathering of original troilite. Notably, this terrestrial pyrrhotite does not contain a peak at 2473.4 eV, demonstrating it is devoid of H-S. As such, the creation of pyrrhotite through terrestrial weathering does not lead to the incorporation of H.

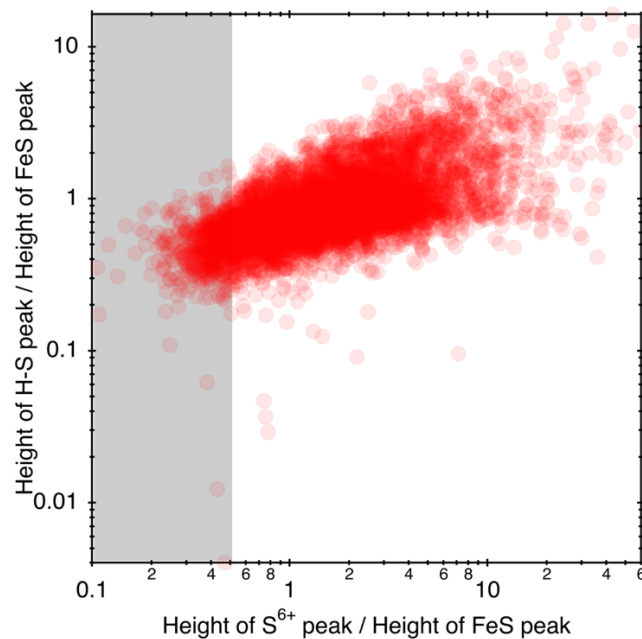


Fig. S5. Plot of the amplitude of H-S peak relative to the FeS peak against the amplitude of S^{6+} peak relative to the FeS peak, in spectra containing detectable H-S peaks. The positive trend can be explained by the fact that FeS is the source of both native H-S, locked in the structure of pyrrhotite, and S^{6+} produced in terrestrial weathering

reactions of FeS. To avoid the influence of terrestrial weathering in our analysis, we limited our calculations to points where S^{6+}/FeS was below 0.5, as shown by the grey box, which isolated only the most pristine points.

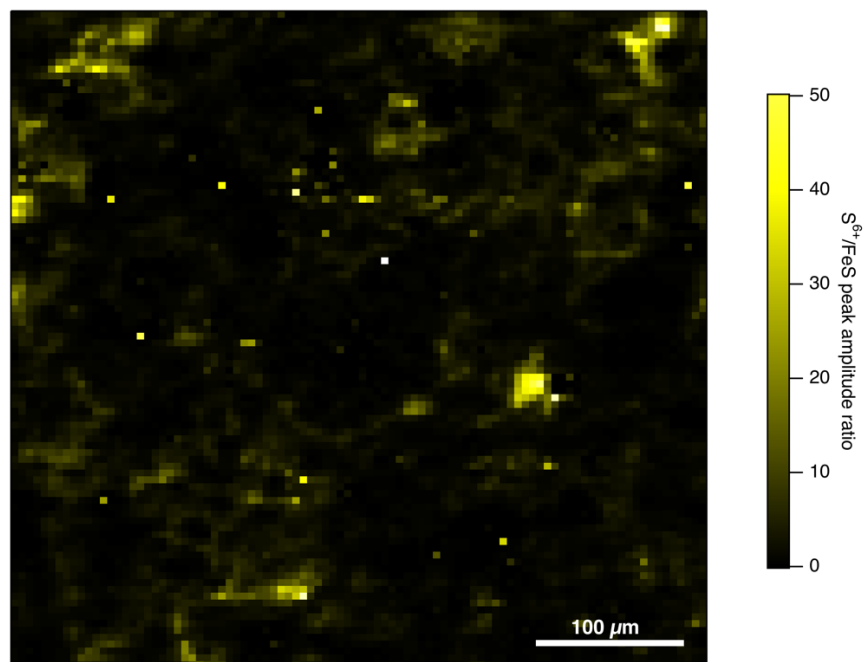


Fig. S6. Map of S^{6+}/FeS peak amplitude across the mapped area. S^{6+} abundance varies widely and is very heterogeneous, indicating that terrestrial weathering products are mostly in situ at the position of the precursor sulfides. The corresponding optical image is shown in Fig 2a.

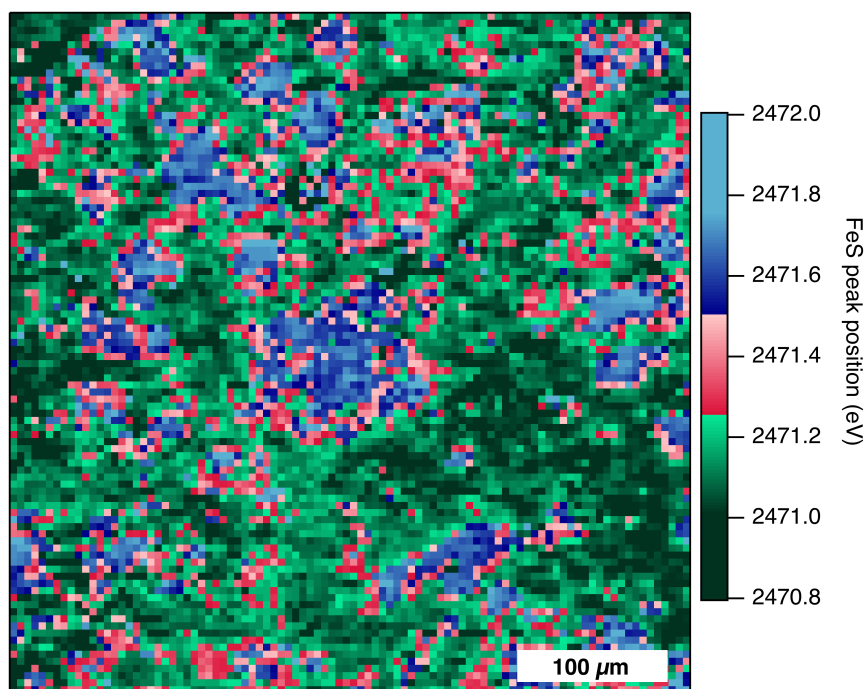


Fig. S7. XANES map showing the peak position of the iron sulfide peak throughout our mapped area. In the center of sulfide grains, the peak is located toward 2472.0 eV, indicating the presence of stoichiometric FeS (troilite). At the rims of these grains and into the matrix material surrounding them, the peak position shifts to lower energy,

indicating that iron sulfides are non-stoichiometric (Head et al., 2018). The corresponding optical image is shown in Fig. 2a.

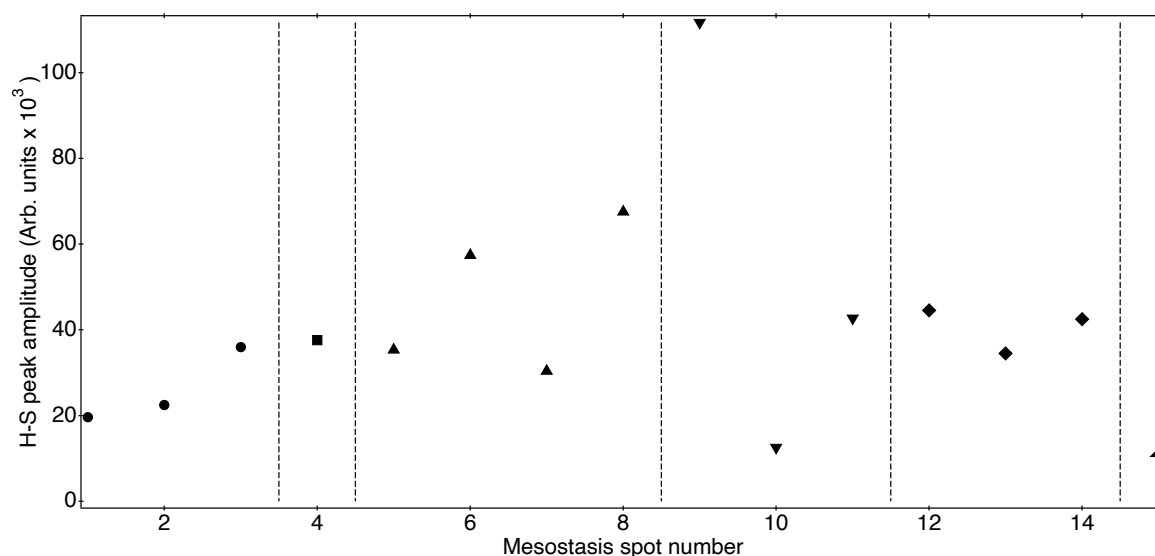


Fig. S8. H-S peak amplitudes taken from 15 spot spectra in chondrule mesostasis across 6 different chondrules. Chondrules are distinguished through different shapes, as well as dashed vertical lines. Measurements in each chondrule were taken from different patches of mesostasis within the chondrule.

Supporting References

- Anzures, B., Parman, S., Milliken, R., Lanzirotti, A., & Newville, M. (2019). XANES Spectroscopy of Sulfides Stable under Reducing Conditions. *American Mineralogist*. <https://doi.org/10.2138/am-2020-7146>
- Bland, P. A., Zolensky, M. E., Benedix, G. K., & Sephton, M. A. (2006). *Weathering of Chondritic Meteorites* (p. 853). <https://ui.adsabs.harvard.edu/abs/2006mess.book..853B>
- Bose, M., Root, R. A., Guan, Y., Eaton, J., Wittmann, A., Skrmetti, T., & Desch, S. J. (2024). Evidence of both molecular cloud and fluid chemistry in Ryugu regolith. *Science Advances*, *10*(30), eadp3037. <https://doi.org/10.1126/sciadv.adp3037>
- Fleet, M. E. (2005). XANES SPECTROSCOPY OF SULFUR IN EARTH MATERIALS. *The Canadian Mineralogist*, *43*(6), 1811–1838. <https://doi.org/10.2113/gscanmin.43.6.1811>
- Head, E., Lanzirotti, A., Newville, M., & Sutton, S. (2018). Vanadium, sulfur, and iron valences in melt inclusions as a window into magmatic processes: A case study at Nyamuragira volcano, Africa. *Geochimica et Cosmochimica Acta*, *226*, 149–173. <https://doi.org/10.1016/j.gca.2018.01.033>
- Lehner, S. W., McDonough, W. F., & Németh, P. (2014). EH3 matrix mineralogy with major and trace element composition compared to chondrules. *Meteoritics & Planetary Science*, *49*(12), 2219–2240. <https://doi.org/10.1111/maps.12391>

- Macke, R. J., Consolmagno, G. J., BRITT, D. T., & HUTSON, M. L. (2010). Enstatite chondrite density, magnetic susceptibility, and porosity. *Meteoritics & Planetary Science*, *45*(9), 1513–1526. <https://doi.org/10.1111/j.1945-5100.2010.01129.x>
- Piani, L., Marrocchi, Y., Rigaudier, T., Vacher, L., Thomassin, D., & Marty, B. (2020). Earth's water may have been inherited from material similar to enstatite chondrite meteorites. *Science*, *369*(6507), 1110–1113. <https://doi.org/10.1126/science.aba1948>
- Rubin, A. E., Griset, C. D., CHOI, B.-G., & WASSON, J. T. (2009). Clastic matrix in EH3 chondrites. *Meteoritics & Planetary Science*, *44*(4), 589–601. <https://doi.org/10.1111/j.1945-5100.2009.tb00754.x>
- Thomassin, D., Piani, L., Villeneuve, J., Caumon, M.-C., Bouden, N., & Marrocchi, Y. (2023). The high-temperature origin of hydrogen in enstatite chondrite chondrules and implications for the origin of terrestrial water. *Earth and Planetary Science Letters*, *616*, 118225. <https://doi.org/10.1016/j.epsl.2023.118225>
- Weisberg, M. K., & Kimura, M. (2012). The unequilibrated enstatite chondrites. *Geochemistry*, *72*(2), 101–115. <https://doi.org/10.1016/j.chemer.2012.04.003>